Supporting Information for

Small-molecule azomethines: organic photovoltaics *via* Schiff base condensation chemistry

*Michiel L. Petrus, Ricardo K. M. Bouwer, Ugo Lafont, Stavros Athanasopoulos, Neil C. Greenham and Theo J. Dingemans**

Delft University of Technology, Faculty of Aerospace Engineering, Kluyverweg 1, 2629 HS Delft, The Netherlands

Dutch Polymer Institute (DPI), P.O. Box 902, 5600 AX Eindhoven, The Netherlands

University of Cambridge, Optoelectronics Group, Cavendish Laboratory, J.J. Thomson Avenue, Cambridge, CB3 0HE, United Kingdom

e-mail: T.J.Dingemans@tudelft.nl

Content

Materials and methods

All chemicals were purchased from commercial sources and used as received unless stated otherwise. 2,5-Thiophenedicarboxaldehyde was purified by vacuum sublimation.

^{1}H NMR and ^{13}C NMR spectra were recorded in $CDCl_3$ using a 400 MHz Bruker WM-400. The recorded spectra were referenced to the solvent ($CDCl_3$: ^{1}H, 7.26 and ^{13}C 77.0 ppm) relative to TMS. The "one-step OPV" reaction was followed by ^{1}H NMR using a 42.5 MHz Magritek Spinsolve benchtop NMR spectrometer. GC-MS analyses were performed on a Shimadzu GC2010 series GC coupled to a MS detector (Shimadzu QP2010S) and equipped with a BPX5 capillary column. The oven was heated from 50-300 °C at a rate of 10 °C min^{-1} using a 1 mL min^{-1} helium gas flow. The sample was injected using an Atas GL Optic 3 inlet which was heated from 50-300 °C in one minute. Mass spectra were generated by electron impact and data was collected over the *m/z* range 45–900. Mass spectra were recorded using a Shimadzu QP2010S with direct injection port. Infrared spectra were obtained with a PerkinElmer Spectrum 100. UV-Vis spectra were recorded using a PerkinElmer Lambda 35 UV-vis spectrometer and photoluminescence spectra were recorded by using a PTI Quantamaster spectrofluorimeter.

Electrochemical measurements

Cyclic voltammetry (CV) was measured using a Metrohm Potentiostat (PGSTAT302N) with platinum working and counter electrodes and a pseudo Ag/Ag^{+} reference electrode. Experiments were performed in an oxygen-free chloroform solution of the molecule with 0.1 M tetrabutylammonium hexafluorophosphate as the electrolyte and measured at a scan rate of 10 mV s^{-1}.

Thermal and calorimetric analysis

Thermogravic analysis (TGA) was performed on a Perkin Elmer Pyris diamond TG/DTA

under a nitrogen atmosphere with a scan rate of 10 °C min^{-1}. Differential scanning calorimetry (DSC) was performed on a Perkin Elmer Sapphire DSC at a heating rate of 20 ˚C min^{-1}.

Computational methods

Gas phase electronic structure calculations have been performed to obtain the optimized geometries of the neutral and protonated forms using the Gaussian 09 program and a split valence 6-31G* basis set.[S1] Molecular orbital plots were obtained with the Avogadro molecular editor software. To assess the influence of the approximations made for the exchange and correlation potential we have tested various hybrid and long-range corrected exchange and correlation functionals including B3LYP, CAM-B3LYP, LC-wPBE and wB97XD. Subsequent vibrational frequency calculations at the same level of theory were performed on the optimised neutral and protonated species to characterize the stationary points and no imaginary frequencies were found. To test the sensitivity of these results on the basis set used we have also performed calculations for larger split valence basis sets with polarized and diffuse orbitals up to 6-311++G**. We find that a larger basis set lowers the HOMO level of both the neutral and protonated species by approximately 0.2-0.3 eV and therefore does not influence the magnitude of the energy shift of the HOMO upon protonation. Excited state energies and oscillator strengths for the vertical transitions have been computed from time-dependent density functional theory (TD-DFT) using the ground state geometries of the neutral and protonated forms. Absorption spectra have been broadened by a Lorentzian with a half-width at half maximum of 0.2 eV.

Device preparation

Solar cells were prepared by covering pre-cleaned ITO patterned glass substrates with PEDOT:PSS (Clevios P, VP Al4083) by spin coating. For the devices with a MoO_x hole transporting layer, MoO_3 was deposited by thermal evaporation under vacuum resulting in a 10 nm thick layer.[S2] The active layer, consisting of **TPA-X-TPA** and fullerene (1:2 by

weight), was spincoated from a chloroform solution (15 mg mL^{-1} total weight) with a thickness 55-65 nm. A 1 nm thick layer of lithium fluoride (LiF) followed by a 100 nm thick aluminium layer were deposited by thermal evaporation under vacuum (~2 10^{-7} mbar). Current-voltage characteristics were recorded in a glovebox using a Keithley 2400 source meter under simulated solar light (1000 W m^{-2}) from a tungsten-halogen lamp filtered by a Schott GG385 UV filter and a Hoya LB120 daylight filter was used to illuminate the devices. Short-circuit currents under AM1.5G conditions were estimated from the spectral response in combination with the solar spectrum. The spectral response was measured under simulated 1 sun operation conditions using bias light from a 532 nm solid state laser (Edmund Optics). Light from a 50 W tungsten halogen lamp (Osram64610) was used as probe light and modulated with a mechanical chopper before passing through a monochromator (Oriel, Cornerstone 130) to select the wavelength. The response was recorded as the voltage over a 50 Ω resistance, using a lock-in amplifier (Stanford Research Systems SR 830). A calibrated Si cell was used as reference. The device was kept behind a quartz window in a nitrogen filled container. The layer thicknesses were measured on a Veeco Dektak 150 profilometer.

Transmission electron microscopy

Transmission electron microscopy (TEM) was performed using a FEI Tecnai TF20 electron microscope operated at 200 kV. The films were spin coated on PEDOT:PSS and transferred to a copper grid.

Synthesis and characterization

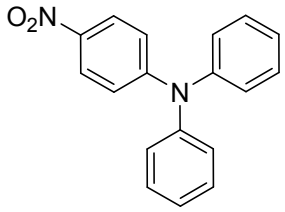

4-nitrotriphenylamine[S3]

A 1 L three-neck flask equipped with stirring bar, condenser and N_2 inlet was charged with diphenylamine (76 g, 0.45 mol), K_2CO_3 (145 g), and DMSO (400 mL). The white suspension was stirred for 30 min at room temperature after which 4-fluoronitrobenzene (70 mL, 0.66 mol) was added in one go. The suspension instantly turned orange. The reaction mixture was heated to 150 °C and stirred at that temperature overnight. The dark reaction mixture was allowed to cool to room temperature and poured onto crushed ice, extracted with DCM. The combined organic layers were dried on $MgSO_4$ and solvent was removed *in vacuo* yielding red solids consisting of a mixture of product and starting compounds. The pure title compound was obtained as an orange solid in 58 % (75 g, 0.26 mol) after subsequent crystallizations from toluene and hexane. ^{1}H-NMR ($CDCl_3$, 400 MHz) δ ppm 8.04 (m, 2H), 7.39 (m, 4H), 7.23 (m, 6H), 6.95 (m, 2H); ^{13}C-NMR ($CDCl_3$, 400 MHz) δ ppm 153.50, 145.66, 140.14, 130.00, 126.57, 125.82, 125.45 and 118.09.

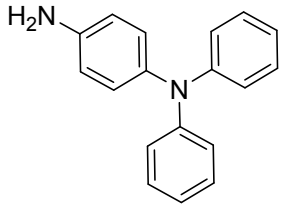

4-aminotriphenylamine (1)[S3]

4-nitrotriphenylamine (3.5 g, 12.1 mmol) was dissolved in dry THF (50 mL) and palladium on carbon (10%, 0.4 g) was added to the reaction mixture. After degassing, the mixture was shaken for 3h under a 4 bar hydrogen atmosphere before filtering over celite. Removing the solvent yielded 3.00 g (11.6 mmol, 96%) of the title compound as a white solid. ^{1}H-NMR ($CDCl_3$, 400 MHz) δ: 7.19 (t, J = 7.7Hz, 4H); 7.04 (d, 8.3Hz, 4H); 6.97-6.89 (m, 4H); 6.61 (d, J = 8.6Hz, 2H); 3.54 (br, 2H); ^{13}C-NMR ($CDCl_3$, 400MHz) δ: 148.2; 143.0; 138.8; 128.9; 127.8; 122.4; 121.4; 116.1; FTIR: 3351, 3033, 1582, 1508, 1486, 1329, 1264, 821, 749 cm^{-1}; MS *m/z* (relative intensity): 261.05 (19%), 260.10 (100), 259.15 (17), 130.05 (13)

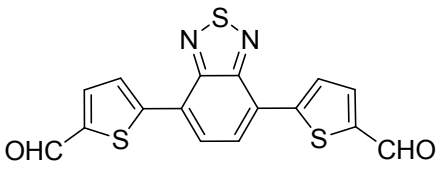

4,7-bis(5-formylthiophen-2-yl)-2,1,3-benzothiadiazole (2b)[S4]

All solvents were degassed before use. In a dry 3-necked flask under argon, 4,7-dibromo-2,1,3-benzothiadiazole (2.0 g, 6.8 mmol) and $PdCl_2(PPh)_3$ (560 mg,) are dissolved in benzene (100 mL). 5-formylthiophene-2-ylboronic acid (3.2 g, 20.5 mmol) in ethanol (48 mL) was added followed by a Na_2CO_3 solution (2M, 48 mL). The mixture was heated to 50 °C and turns orange with a white precipitate. After 5h, the mixture was allowed to cool to room temperature and the solids were filtered off. The residue was washed with water (3x 100 mL), MeOH (3x 100 mL) and chloroform (3x 100 mL), resulting in the title compound as an orange solid (2.2 g, 90%). The product was further purified by crystallization from chloroform (~100 mg/L). Mp: 330 ˚C; FTIR: 3083, 2844, 1638, 1442, 1221, 814, 757, 670 cm^{-1}; GC-MS *m/z* (relative intensity): T_r = 37 min. 356.0 (100%), 355.0 (34), 45.1 (26), 357.0 (24), 69.0 (16), 266 (14)

TPA-Th-TPA (3a)

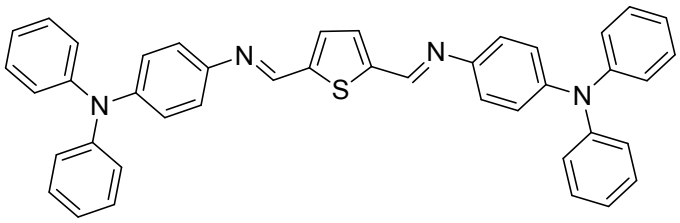

4-aminotriphenylamine (1.7 g, 6.5 mmol) and 2,5-thiophenecarboxaldehyde (0.42 g, 3.0 mmol) were placed in a dry round-bottom flask with condenser under nitrogen atmosphere. Dry chloroform (40 mL) and dry isopropanol (20 mL) were added, followed by a crystal of *p*-toluenesulfonic acid as a catalyst. The mixture turned orange and was heated to reflux. After 3 days the mixture is cooled to room temperature and the orange precipitate was filtered off. The product was washed by isopropanol and isopropanol:triethylamine (98:2) resulting in 1.85 g (98%, 2.9 mmol) of the

title compound. Mp 208 °C, ^{1}H-NMR ($CHCl_3$, 400MHz) δ: 8.59 (s, 2H); 7.43 (s, 2H); 7.26 (t, 8H); 7.19 (d, 4H); 7.12-7.07 (m, 12H); 7.03 (t, 4H); ^{13}C-NMR ($CHCl_3$, 100MHz) δ:150.2; 147.6; 146.7; 146.4; 145.2; 131.3; 129.3; 124.4; 124.3; 123.0; 122.3; FTIR: 3034, 1587, 1489,1314, 1279, 830, 751, 694, 620 cm^{-1}; MS *m/z* (relative intensity): 624.15 (100%); 625.15 (47); 312.15 (91); 167.05 (30); 77.05 (24)

TPA-TBT-TPA (3b)

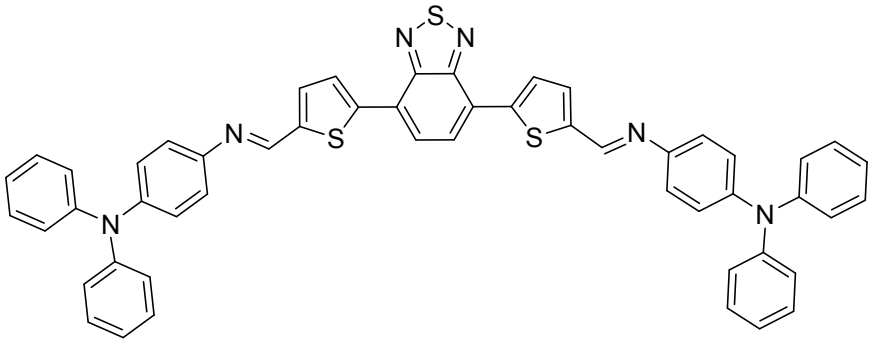

TPA-TBT-TPA was obtained by a similar procedure as described for **TPA-Th-TPA**, starting from 4-aminotriphenylamine (0.87 g, 3.4 mmol) and 4,7-bis(5-formylthiophen-2-yl)-2,1,3-benzothiadiazole (0.50 g; 1.4 mmol) stirring in chloroform only (40 mL) at reflux. After cooling to room temperature isopropanol was added to precipitate the product he solids were filtered off and washed with isopropanol and isopropanol:triethylamine (98:2), resulting in a dark purple solid (1.04 g, 1.2 mmol, 88%). Mp 248 °C, ^{1}H-NMR (C_6D_6, 400MHz) δ: 8.32 (s, 2H); 8.12 (d, 2H); 7.38 (s, 2H); 7.20-7.04 (m, 26H); 6.86 (t, 4H); ^{1}H-NMR ($CHCl_3$ aggregates at >10 mg/mL, 400MHz) δ: 8.84 (s, 2H); 8.23 (d, 2H); 7.99 (s, 2H); 7.53 (d, 2H); 7.29-7.22 (m, 12) 7.13-7.10 (m, 12H); 7.03 (t, 4H); ^{13}C-NMR (C_6D_6, 100MHz) δ: 152.4; 150.4; 148.1; 146.7; 146.2; 144.6; 143.4; 132.3; 129.5; 128.5; 126.1; 126.0; 124.8; 124.5; 123.0; 122.7; FTIR: 3032, 1585, 1487, 1270, 837, 825, 811, 749, 690, 615 cm^{-1};

Preparation of **TPA-Th-TPA (3a)** for the one-step OPV fabrication

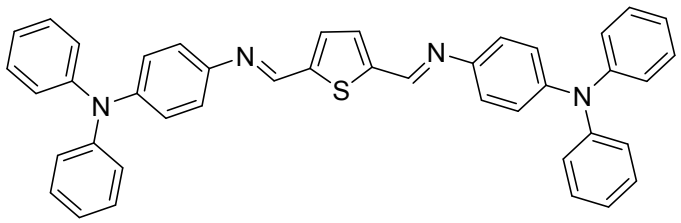

4-aminotriphenylamine (41 mg, 2 eq.) and 2,5-thiophenecarbaldehyde (11 mg, 1 eq) were placed in a dried flask under nitrogen atmosphere. Dry chloroform (1 mL) was added the mixture turned orange within seconds and was stirred at 60 °C overnight. The reaction was followed by performing the same reaction in dry $CDCl_3$. NMR showed that after one night the conversion is approximately 99%. The reaction mixture was diluted 10 times and to 1 mL of the solution, 10 mg [70]PCBM was added. This solution was used for spincoating in the same procedure as the other solutions.

Thermal properties

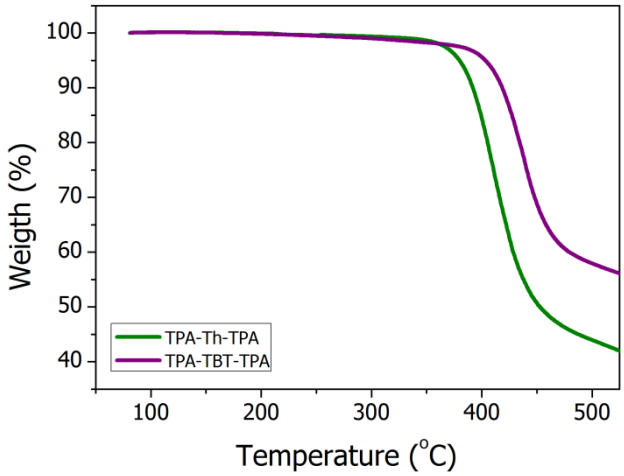

Figure S1. TGA thermograms of the **TPA-X-TPA** small molecules at a heating rate of 10 °C min^{-1} under nitrogen.

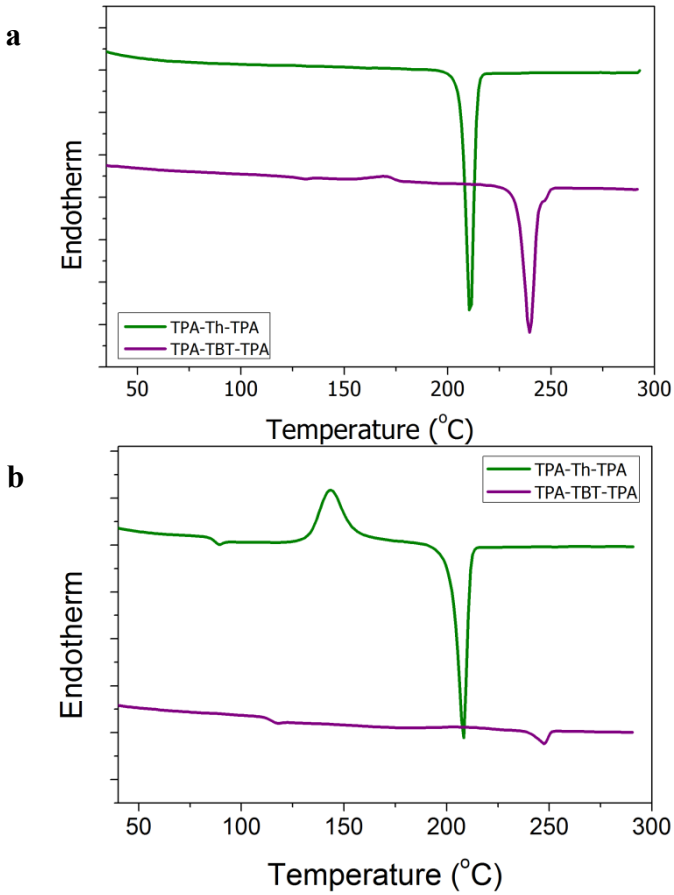

Figure S2. Normalized DSC curves for the **TPA-X-TPA** small molecules. **a,** 1st heat, showing sharp melting exotherms. **b,** 2nd heat clearly showing the glass transition temperature (Tg), cold crystallization and melt transitions.

Table S1. Summary of the thermal properties of **TPA-X-TPA.**

Compound	T_g (°C)[a]	T_{cryst} (°C)[b]	T_m (°C)[b]	T_d (°C)[c]
TPA-Th-TPA	86	143	208	380
TPA-TBT-TPA	114	-	248	403

[a] Glass transition (Tg) recorded at the inflection point in the DSC curve at a heating rate of 20 °C min^{-1}; [b] Peak maximum in DSC curve at a heating rate of 20 °C min^{-1}; [c] Temperature at a thermal decomposition of 5% measured by TGA at a heating rate of 10 °C min^{-1}.

Optical properties

UV Vis spectra

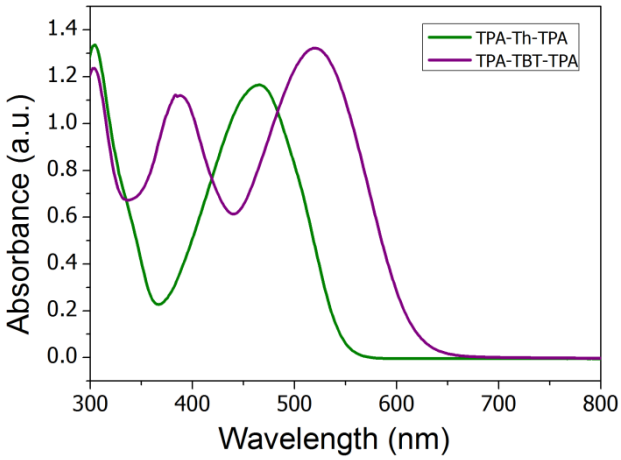

Figure S3. UV-Vis absorption spectrum of **TPA-X-TPA** azomethines at a concentration of 20 mg/L in dichloromethane.

Halochromatic behaviour

Azomethines are known to be halochromatic, which results in significant change in their absorption spectrum upon protonation.[S5,S6,S7] Addition of 1 or 2 equivalent of *para*-toluene sulfonic acid (pTSA) to the azomethine solutions resulted in a visible colour change and a red shift in the absorption spectrum. For the **TPA-Th-TPA** a new absorption maximum at 615 nm is observed (shift of 148 nm), which is attributed the protonated small molecule. Upon

addition of 2 equivalents the intensity of the absorption maximum at 615 nm further increases while the absorption of the neutral species further decreases. In addition an extra absorption band appears around 850 nm.

For **TPA-TBT-TPA** the absorption maximum was red shifted from 520 to 575 nm upon addition of 2 equivalents of pTSA. Also a decrease of the absorption maximum at 389 nm and 520 nm was observed upon addition of acid. A similar colour change of the solution was also observed, although to a lesser extent, when the small molecules were dissolved in acidic solvents like $CHCl_3$.

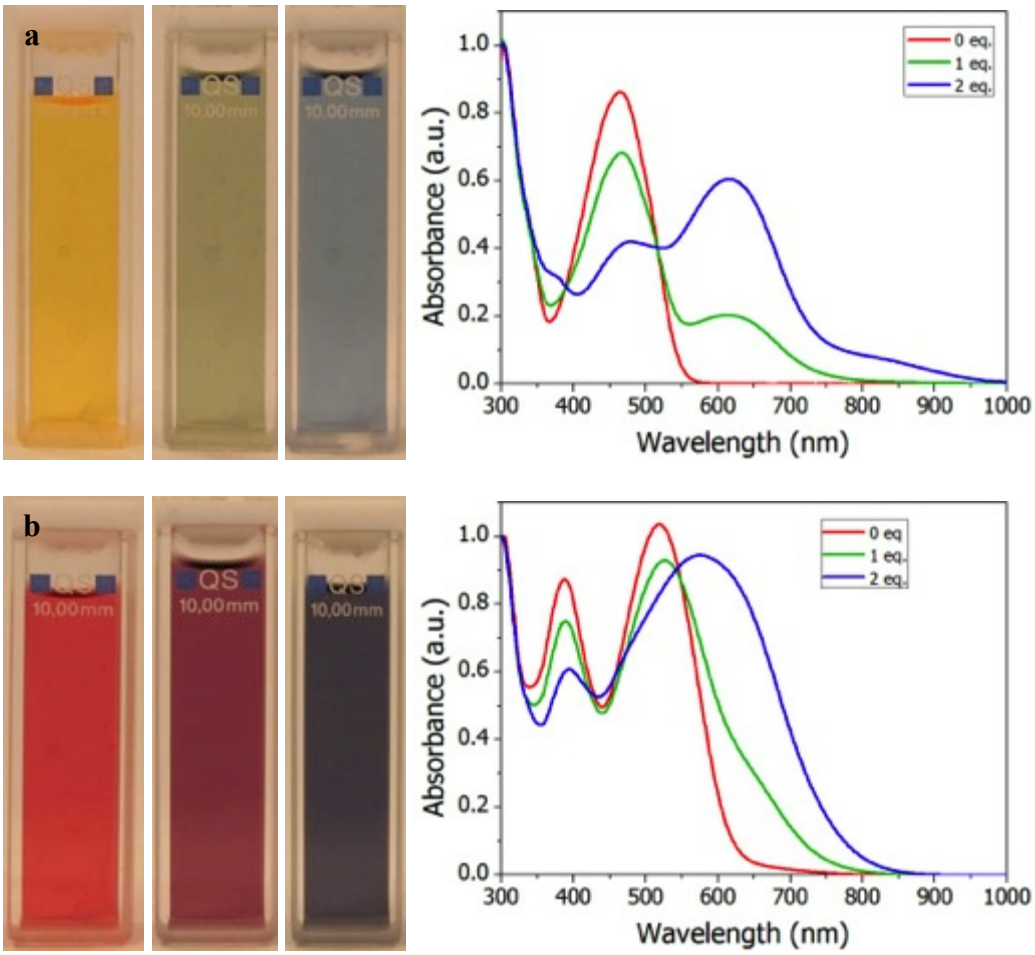

Figure S4. Halochromatic behaviour of **TPA-Th-TPA** and **TPA-TBT-TPA** in dichloromethane upon addition of *p*-toluenesulfonic acid. Series **a** shows **TPA-Th-TPA**, with, from left to right, 0 (neutral), 1 and 2 equivalents of pTSA and their UV-Vis absorption spectra. Series **b** shows **TPA-TBT-TPA**, with, from left to right, 0 (neutral), 1 and 2 equivalents of pTSA, and their UV-Vis absorption spectra.

Photoluminescence Spectra

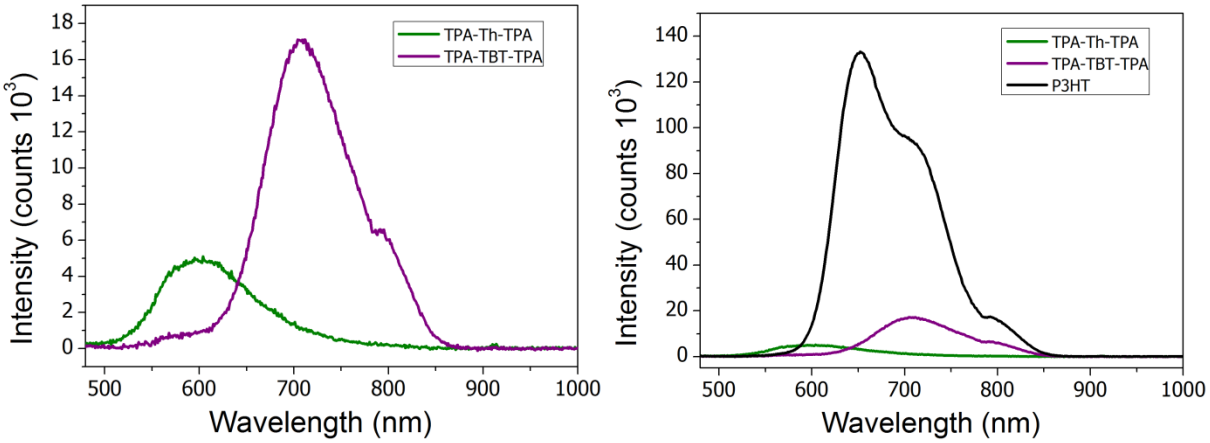

Figure S5. Room temperature photoluminescence spectra of **TPA-X-TPA** small molecules in the solid state. The photoluminescence of the small molecules compared to P3HT, which is a weak photoluminescence material itself, showing that the PL is very weak for these azomethines. The materials were excited at 440 nm.

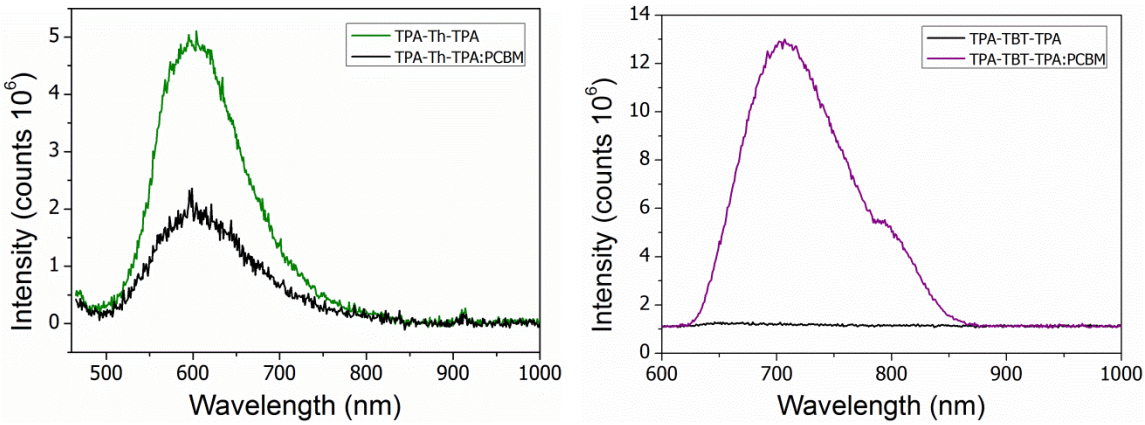

Figure S6. Photoluminescence quenching data for **TPA-X-TPA**:[60]PCBM blend films. **TPA-Th-TPA** was excited at 440 nm while **TPA-TBT-TPA** was excited at 550 nm. The residual luminescence of the **TPA-Th-TPA**:PCBM blend with a maximum at 600 nm is ascribed to [60]PCBM.

Table S2. Summary of the photoluminescence of **TPA-X-TPA.**

Compound	λ_{max} **(nm)**[a]
TPA-Th-TPA	590
TPA-TBT-TPA	700

[a] measured in the solid state.

Electronic properties

Cyclic Voltammetry

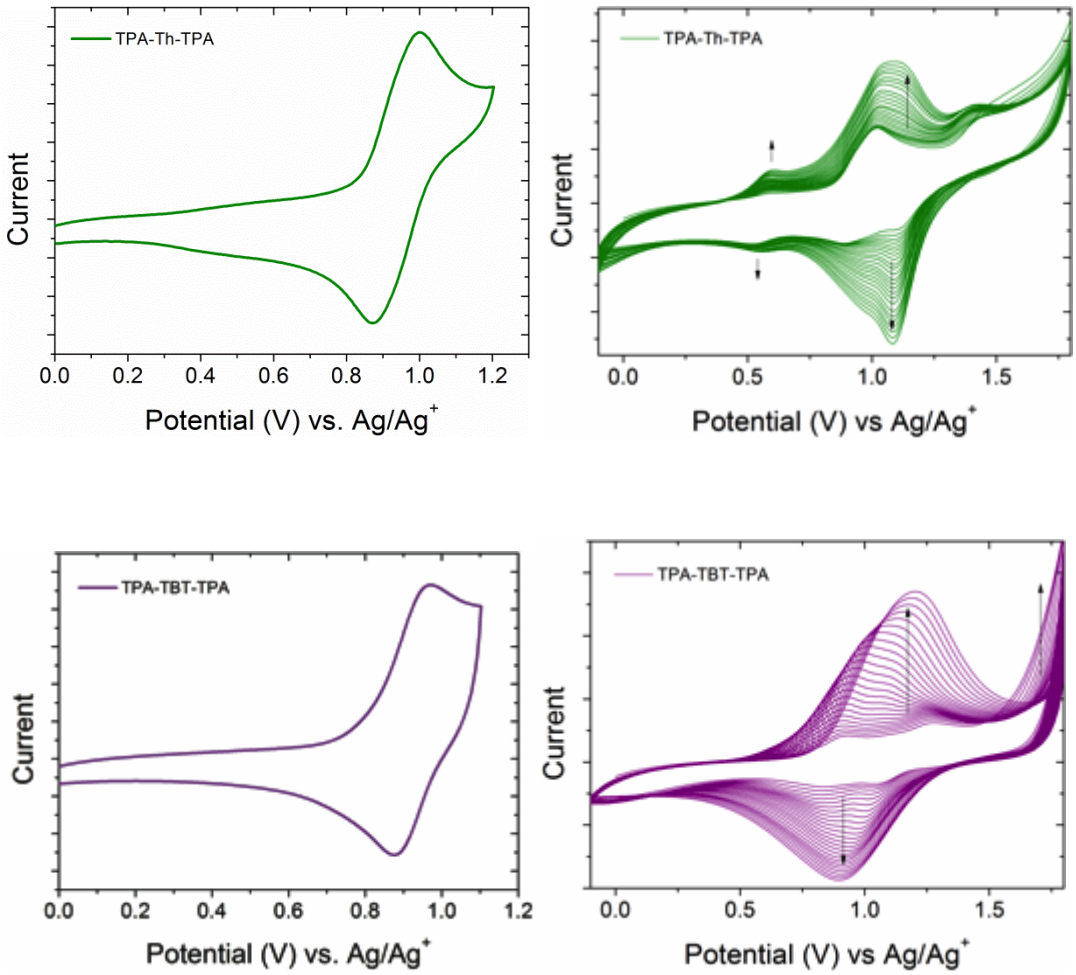

Figure S7. Cyclic voltammetry diagram of the oxidation behaviour of the **TPA-X-TPA** small molecules. Measured in dichloromethane with 0.1 M $TBAPF_6$ at a scan rate of 100 mV/s, potential vs. Ag/Ag^+. On the left the reversible 1st oxidation, on the right cyclic oxidation and reduction to neutral species over 25 cycles, resulting in new species with new oxidation and reduction behaviour.

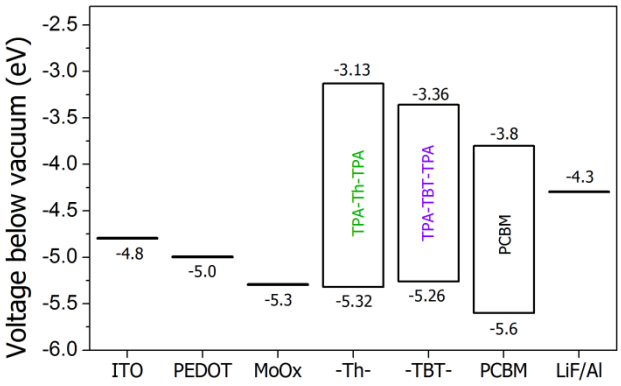

Figure S8. Energy level diagram of the different **TPA-X-TPA** small molecules, [60]PCBM and the electrodes work function.

Computational study

As already indicated by their halochromatic behaviour, azomethines are easily protonated in acid media.[S5,S8] To study the effect of protonation and to see whether the protonated azomethines might form an insulating layer at the PEDOT-PSS/active layer interface a computational study was performed. Density functional theory (DFT) calculations were carried out to studied the effect of protonation of the azomethine nitrogen and also for the TPA nitrogen site.[1] **TPA-Th-TPA** was chosen as a representative example of the small molecule azomethines. DFT calculations obtained from various exchange and correlation functionals are consistent and indicate that protonation of the azomethine nitrogen breaks the symmetry and enforces localization of the highest occupied molecular orbital (HOMO) to the non-protonated part of the molecule resulting in a lowering of the HOMO energy by approximately ~2 eV (Figure 2) while the LUMO level shows a downward shift in energy by more than 3 eV. This suggests that, upon protonation of the azomethine molecules at the PEDOT:PSS interface, energy barrier states for holes and well states for electrons are formed. This can be detrimental for hole extraction and can also lead to enhanced recombination. Similar conclusions in terms of localization and a downward shift of the HOMO energies were reached when the TPA nitrogen was protonated (Figure S9). However, we found that

protonation of the TPA moiety as compared to the azomethine nitrogen site is energetically less favourable.

The absorption spectra of the neutral, protonated and double protonated **TPA-Th-TPA** were calculated at the TD-TFT level and are displayed in Figure S13. Single protonation of the azomethine results in a large red shift which is comparable with red shift observed in the experimental data shown in Figure S4. Protonation of both azomethines shifts the absorption further to the red. This double protonation explain the extra absorption band around 850 nm that appears upon addition of two equivalents of acid. Overall, the computational data on the protonation-induced changes in absorption energies are in agreement with the experimental data which supports the predicted influence of protonation on the electronic structure of the azomethine molecules.

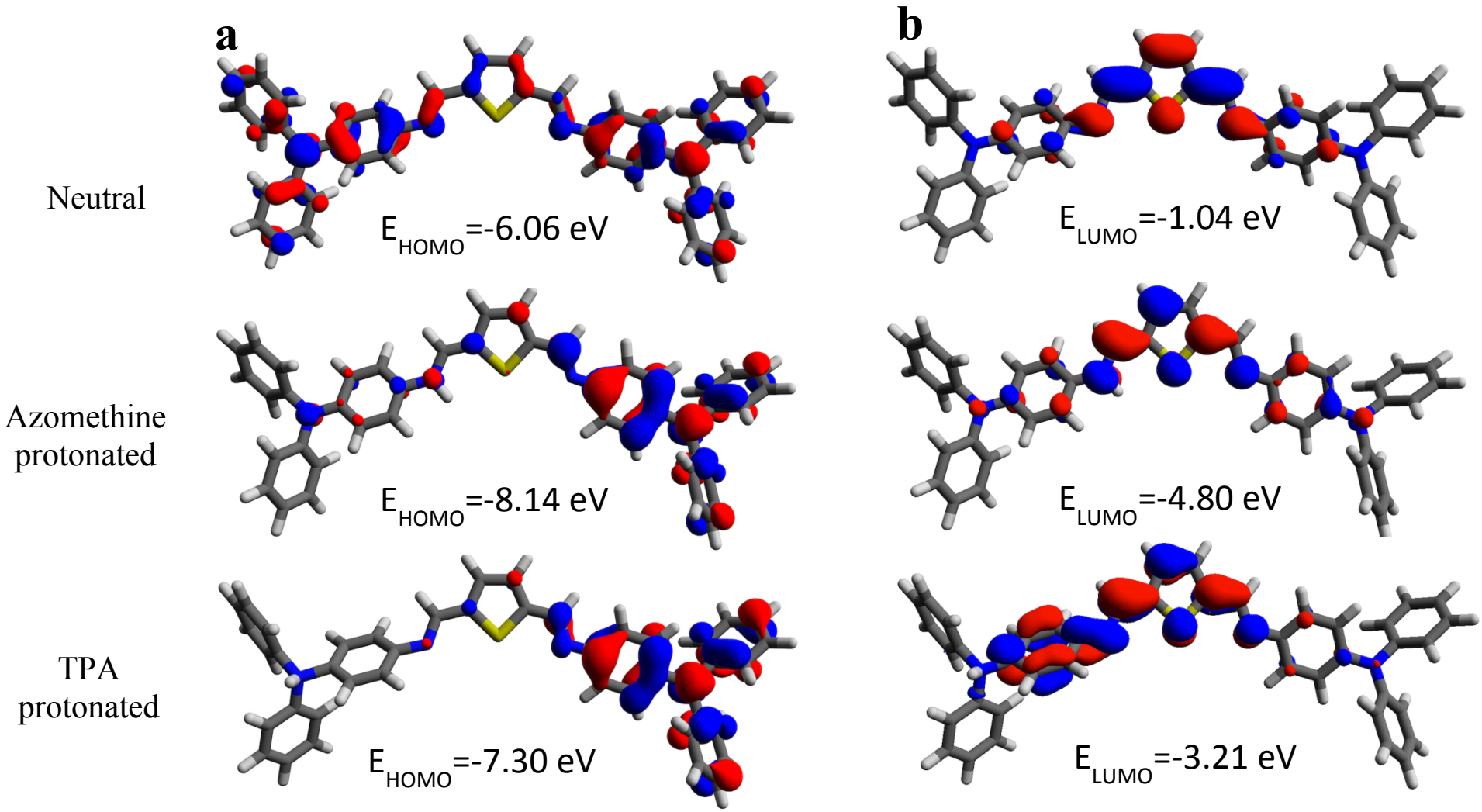

Figure S9: Frontier molecular orbital distributions and energies. Kohn-Sham HOMO (**a**) and LUMO (**b**) at the CAM-B3LYP/6-31G* level for the TPA-Th-TPA molecule. Top panels: neutral state; middle panels: azomethine nitrogen protonated state; bottom panels: triphenylamine nitrogen protonated state. In both cases protonation results in a localization of the HOMO.

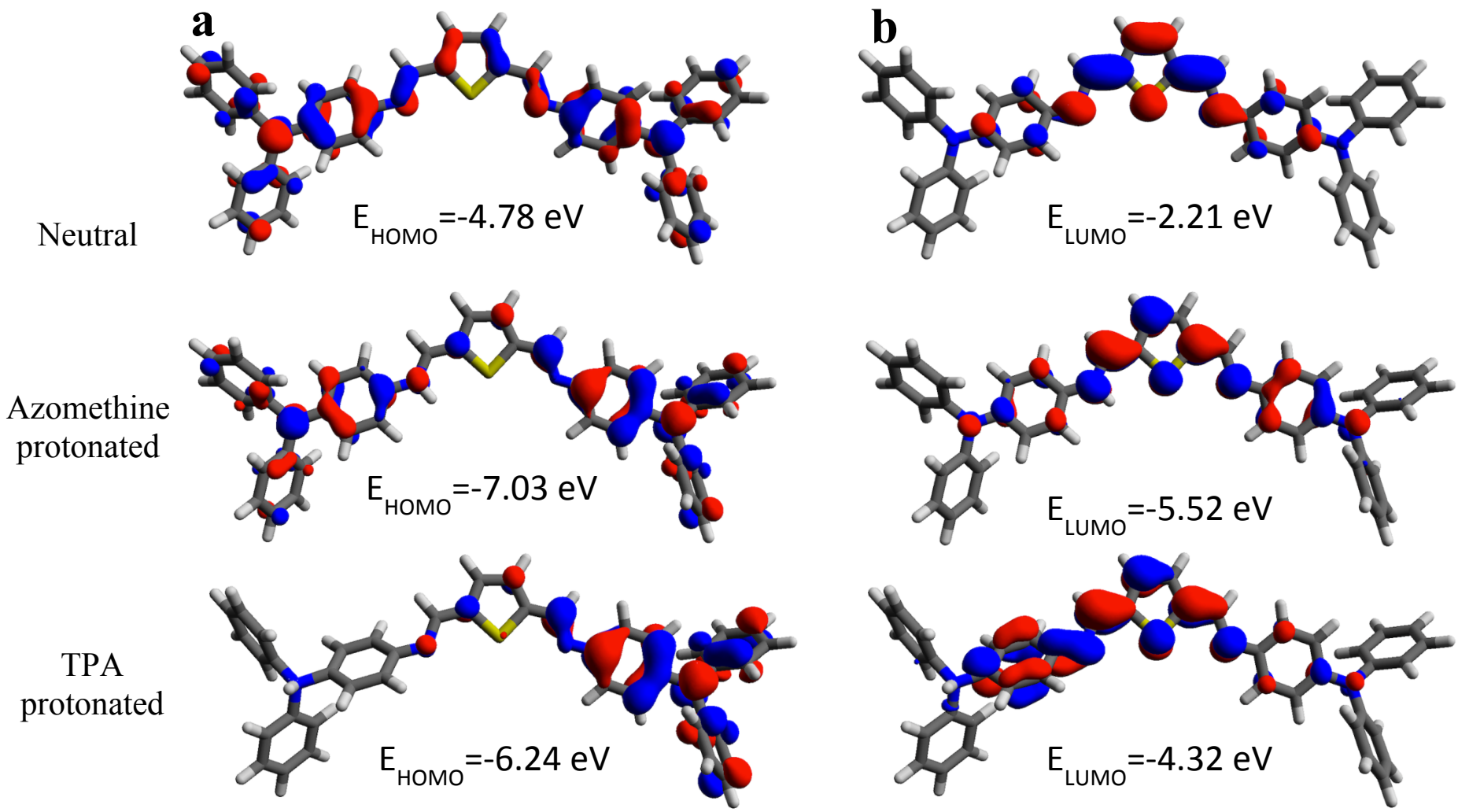

Figure S10: Frontier molecular orbital distributions and energies. Kohn-Sham HOMO (**a**) and LUMO (**b**) at the B3LYP/6-31G* level for the TPA-Th-TPA molecule. Top panels: neutral state; middle panels: azomethine nitrogen protonated state; bottom panels: triphenylamine nitrogen protonated state. In both cases protonation results in a localization of the HOMO.

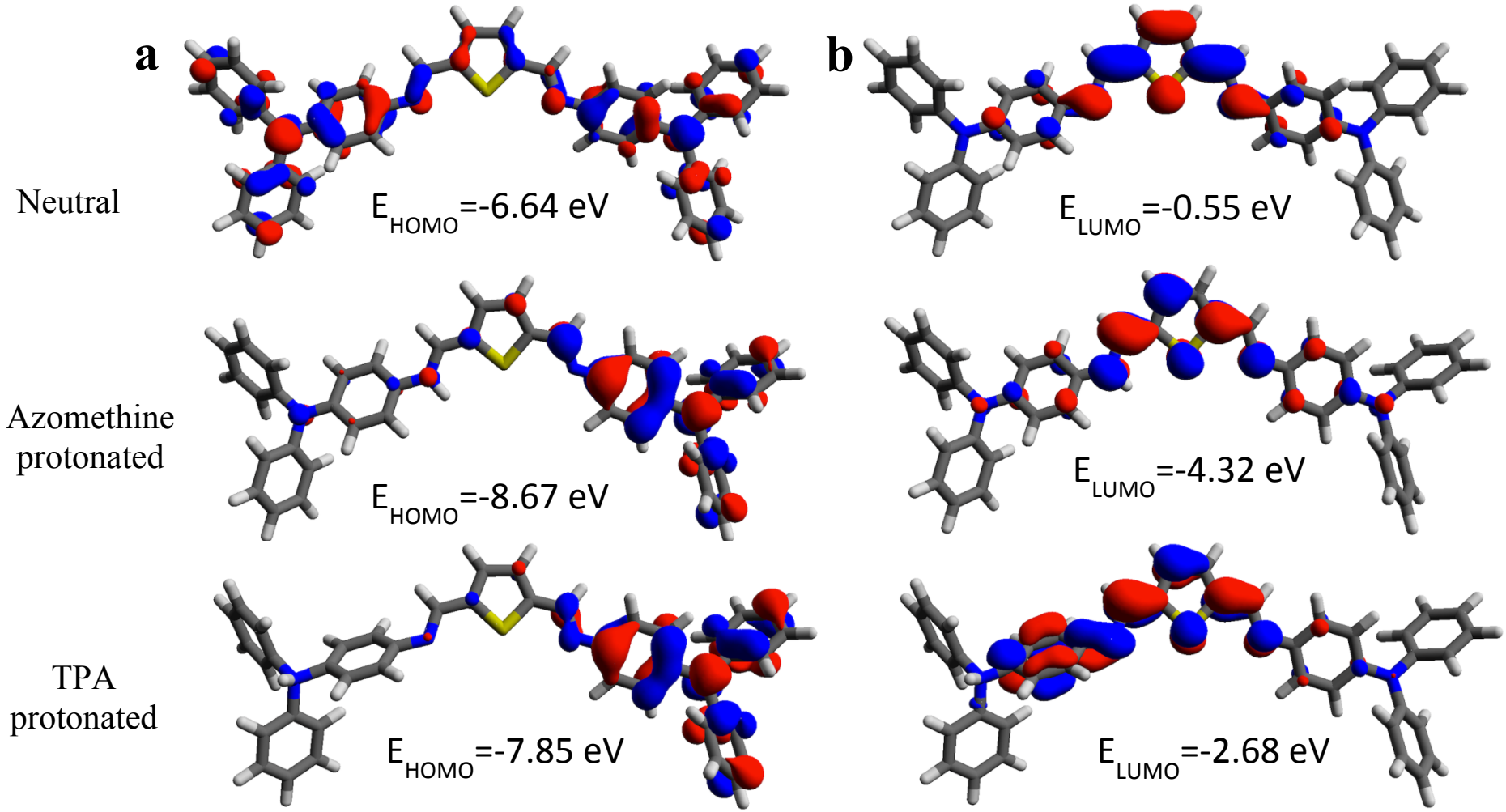

Figure S11: Frontier molecular orbital distributions and energies. Kohn-Sham HOMO (**a**) and LUMO (**b**) at the wB97XD/6-31G* level for the TPA-Th-TPA molecule. Top panels: neutral state; middle panels: azomethine nitrogen protonated state; bottom panels: triphenylamine nitrogen protonated state. In both cases protonation results in a localization of the HOMO.

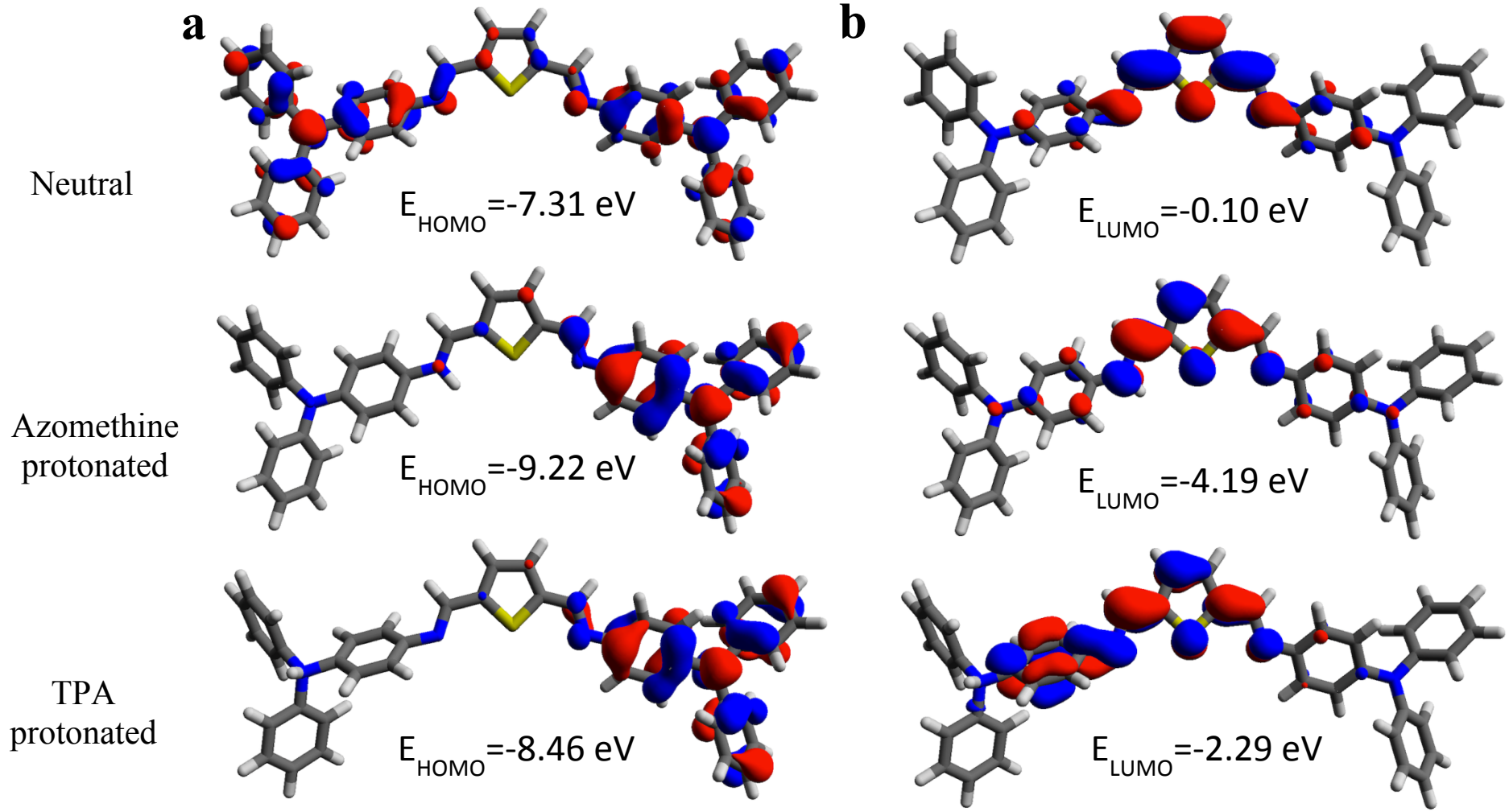

Figure S12: Frontier molecular orbital distributions and energies. Kohn-Sham HOMO (**a**) and LUMO (**b**) at the LC-wPBE/6-31G* level for the **TPA-Th-TPA** molecule. Top panels: neutral state; middle panels: azomethine nitrogen protonated state; bottom panels: triphenylamine nitrogen protonated state. In both cases protonation results in a localization of the HOMO.

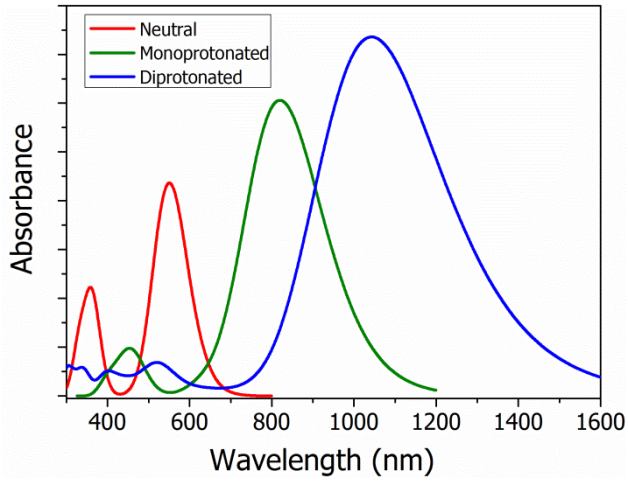

Figure S13: Absorption spectra calculated at the B3LYP/6-31G* level for the **TPA-Th-TPA** molecule in vacuum. Red: absorption spectrum in the neutral state; green: single protonated azomethine; blue: double protonated azomethine.

Photovoltaic device characteristics

Table S3. Studying the hole-collecting layer (HCL) in photovoltaic devices with ITO/HCL/**TPA-TBT-TPA**:[60]PCBM(1:2)/LiF/Al configurations

Hole blocking layer	J_{sc} (mA cm^{-2})	V_{oc} (V)	FF (%)	MPP (%)
PEDOT-PSS	2.31	0.45	34	0.35
MoO_x	2.18	0.68	28	0.42

Table S4. Studying annealing time in photovoltaic devices with ITO/MoO_x/**TPA-TBT-TPA**:[60]PCBM(1:2)/LiF/Al configurations at 70 °C.

Total anneal time (min)[a]	J_{sc} (mA cm^{-2})	V_{oc} (V)	FF (%)	MPP (%)
0	2.18	0.68	28	0.42
5	2.28	0.76	33	0.57
15	2.33	0.76	33	0.59
30	2.35	0.77	34	0.62
60	2.37	0.78	35	0.65
120	2.38	0.78	35	0.65

[a] The data were obtained by subsequently heating the device while measuring the device characteristics after the given total annealing times.

Table S5. Studying acceptor in photovoltaic devices with ITO/MoO_x/**TPA-TBT-TPA**:PCBM(1:2)/LiF/Al configurations after annealing at 70 °C.

Acceptor	J_{sc} (mA cm^{-2})[a]	V_{oc} (V)	FF (%)	PCE (%)
[60]PCBM	2.66	0.81	34	0.73
[70]PCBM	4.50	0.75	34	1.15

[a] J_{sc} was calculated by integrating the EQE spectrum with the AM1.5G spectrum measured under light bias. MPP was calculated using the current which was not corrected for the AM1.5G spectrum. PCE were calculated using the corrected currents.

The optimal annealing time was found to depend on both the donor and acceptor material. Annealing at 70 °C resulted in an increase in efficiency for all devices; the optimum annealing time was found by subsequently heating the device while measuring the device characteristics. Annealing temperatures of 100 °C and higher resulted in a decrease in efficiencies.

Table S6. Optimal annealing time at 70 °C for devices with ITO/MoO_x/**TPA-X-TPA**:PCBM(1:2)/LiF/Al configuration.

Donor	Acceptor	Time (min)
TPA-TBT-TPA	[60]PCBM	60
TPA-TBT-TPA	[70]PCBM	5
TPA-Th-TPA	[70]PCBM	30

***J-V* curves**

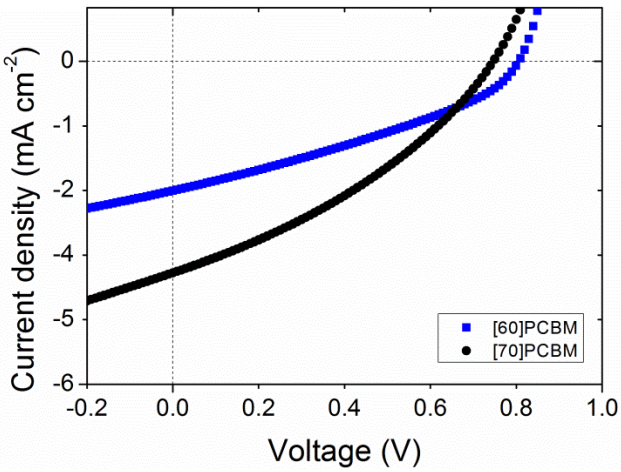

Figure S14. *J-V* curve of **TPA-TBT-TPA**:PCBM devices using [60]PCBM and [70]PCBM. [70]PCBM shows a significant higher current, leading to higher PCE.

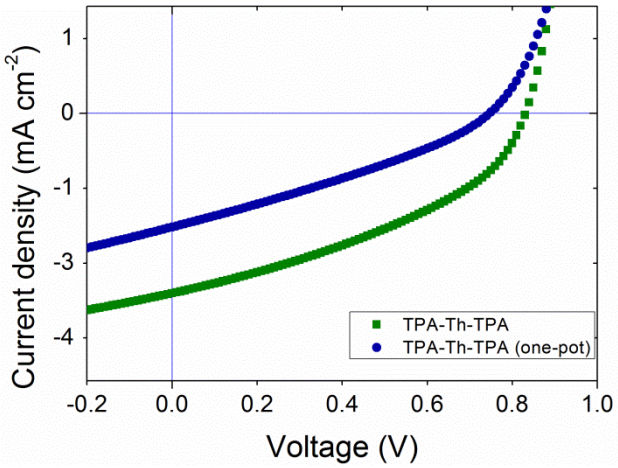

Figure S15. *J-V* curve of **TPA-Th-TPA** (one-pot):[70]PCBM compared to **TPA-Th-TPA**:[70]PCBM prepared via the original method.

Transition Electron Microscopy

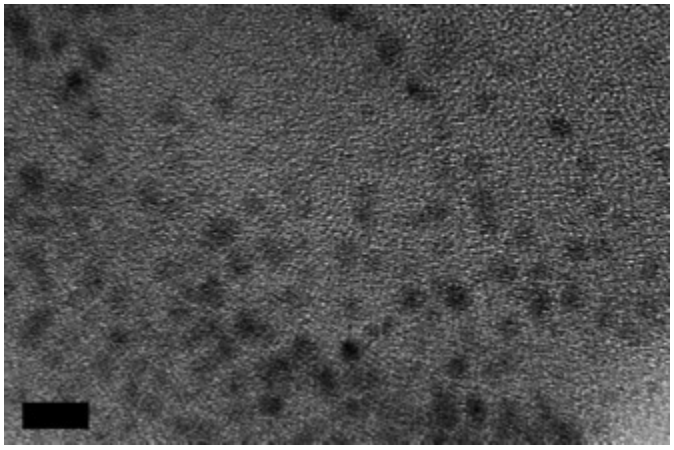

Figure S16. High-magnification TEM image. Image of the nano morphology of **TPA-Th-TPA**:[70]PCBM (1:2) as representative example for the small molecules. The dark areas are the PCBM rich clusters, which are on the length scale of ~2–3 nm. Scale bar shown in bottom left corner: 10 nm.

External quantum efficiencies (EQE)

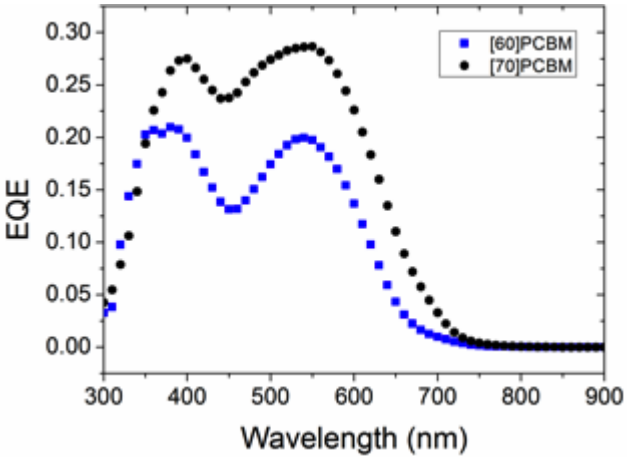

Figure S17. EQE curves of **TPA-TBT-TPA**:PCBM devices using [60]PCBM and [70]PCBM. The higher EQE of [70]PCBM is ascribed to the absorbance of [70]PCBM.

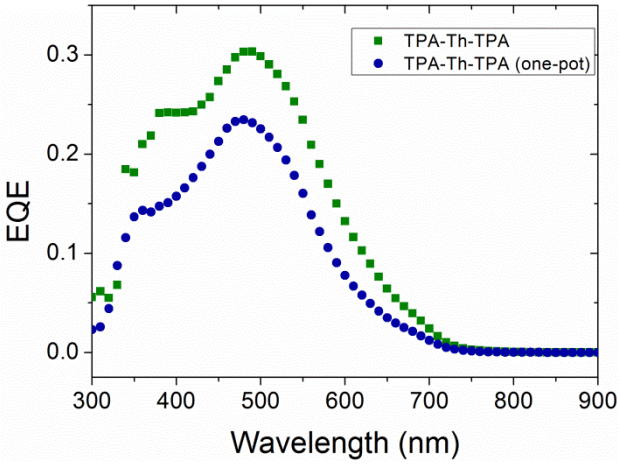

Figure S18. EQE curves of **TPA-Th-TPA (**one-pot OPV synthesis):[70]PCBM compared to **TPA-Th-TPA**:[70]PCBM prepared via the original method.

References

1. M. J. Frisch, G. W. Trucks, H. B. Schlegel, G. E. Scuseria, M. A. Robb, J. R. Cheeseman, G. Scalmani, V. Barone, B. Mennucci, G. A. Petersson, H. Nakatsuji, M. Caricato, X. Li, H. P. Hratchian, A. F. Izmaylov, J. Bloino, G. Zheng, J. L. Sonnenberg, M. Hada, M. Ehara, K. Toyota, R. Fukuda, J. Hasegawa, M. Ishida, T. Nakajima, Y. Honda, O. Kitao, H. Nakai, T. Vreven, J. J. A. Montgomery, J. E. Peralta, F. Ogliaro, M. Bearpark, J. J. Heyd, E. Brothers, K. N. Kudin, V. N. Staroverov, T. Keith, R. Kobayashi, J. Normand, K. Raghavachari, A. Rendell, J. C. Burant, S. S. Iyengar, J. Tomasi, M. Cossi, N. Rega, J. M. Millam, M. Klene, J. E. Knox, J. B. Cross, V. Bakken, C. Adamo, J. Jaramillo, R. Gomperts, R. E. Stratmann, O. Yazyev, A. J. Austin, R. Cammi, C. Pomelli, J. W. Ochterski, R. L. Martin, K. Morokuma, V. G. Zakrzewski, G. A. Voth, P. Salvador, J. J. Dannenberg, S. Dapprich, A. D. Daniels, O. Farkas, J. B. Foresman, J. V. Ortiz, J. Cioslowski, and F. D. J., 2010.

2. Y. Sun, C. J. Takacs, S. R. Cowan, J. H. Seo, X. Gong, A. Roy, and A. J. Heeger, *Adv. Mater.*, 2011, **23**, 2226–2230.

3. M. L. Petrus, R. K. M. Bouwer, U. Lafont, D. H. K. Murthy, R. J. P. Kist, M. L. Böhm, Y. Olivier, T. J. Savenije, L. D. a. Siebbeles, N. C. Greenham, and T. J. Dingemans, *Polym. Chem.*, 2013, **4**, 4182–4191.

4. X. Zhang, R. Yamaguchi, K. Moriyama, M. Kadowaki, T. Kobayashi, T. Ishi-i, T. Thiemann, and S. Mataka, *J. Mater. Chem.*, 2006, **16**, 736–740.

5. S. Barik, T. Bletzacker, and W. G. Skene, *Macromolecules*, 2012, **45**, 1165–1173.

6. A. Bolduc, L. Rivier, S. Dufresne, and W. G. Skene, *Mater. Chem. Phys.*, 2012, **132**, 722–728.

7. H. Niu, J. Cai, P. Zhao, C. Wang, X. Bai, and W. Wang, *Dye. Pigm.*, 2013, **96**, 158–169.

8. J. Gąsiorowski, E. D. Głowacki, B. Hajduk, M. Siwy, M. Chwastek-ogierman, J. Weszka, H. Neugebauer, and N. S. Sariciftci, *J. Phys. Org. Chem. C*, 2013, **117**, 2584–2589.